Journal of Alloys and Compounds 509 (2011) 4510–4515

Contents lists available at ScienceDirect

Journal of Alloys and Compounds

journal homepage: www.elsevier.com/locate/jallcom

Effect of Eu doping on structural and magneto-electrical properties of $La_{0.7}Ca_{0.3}MnO_3$ manganites

S.P. Altintas[a], A. Amira[b], N. Mahamdioua[b], A. Varilci[a], C. Terzioglu[a,*]

[a] Department of Physics, Faculty of Arts and Sciences, Abant Izzet Baysal University, 14280 Bolu, Turkey
[b] LEND, Université de Jijel, B.P. 98 Jijel 18000, Algeria

ARTICLE INFO

Article history:
Received 24 November 2010
Received in revised form 3 January 2011
Accepted 4 January 2011
Available online 6 January 2011

Keywords:
Lanthanum based manganites
Magnetoresistance (MR)
Metal–insulator transition
Doping

ABSTRACT

We have investigated the influence of europium (Eu) doping on structural and magneto-electrical properties of $La_{0.7}Ca_{0.3}MnO_3$ compounds. In order to analyze the physical mechanism of a spin disorder system and study their relative evolutions, two samples of nominal compositions $(La_{0.7-x}Eu_x)Ca_{0.3}MnO_3$ ($x = 0.0$ and 0.1) have been elaborated and characterized. In addition to structural changes seen by this kind of doping, the magnetoresistance (MR) and resistivity are increased while the metal–insulator transition temperature is decreased. Comparing the experimental data with the theoretical models shows that in the metal-ferromagnetic region, the electrical behaviour of both samples is quite well described by a theory based on Kondo-like spin dependent scattering, electron–electron scattering, electron–phonon and electron–magnon scatterings. For the high temperature paramagnetic insulating regime, the adiabatic small polaron hopping model is found to fit well the experimental curves.

1. Introduction

In the past few decades, $AMnO_3$ perovskite-type manganites have been extensively analyzed because of their rich electrical transport and magnetic properties [1–3]. Considerable attention has been exposed from not only academic research but also magnetic industries. The growth of interest in their properties stems in large part from their wide range of technological applications such as read heads for magnetic information storage, low and high field magnetic sensors and more recently spintronic applications [4–6]. Numerous studies have been devoted in the rare earth manganite perovskite with the series of $(La_{1-x}RE_x)_{2/3}Ca_{1/3}MnO_3$ (RE is trivalent rare earth elements such as Y, Pr, Eu, and Sm) which are exhibiting colossal magnetoresistance (CMR) properties [7,8]. These compounds are Mn^{3+} rich and doping with divalent atoms introduces mixture valency of Mn^{3+} and Mn^{4+} ions that plays a major role in the double exchange (DE) ferromagnetic interaction coupled with metallic resistivity [9]. Double exchange effect is an exchange of electrons from neighboring Mn^{3+} to Mn^{4+} ions through oxygen when their core spin are parallel. The hopping is not favored when they are anti-parallel. Although, more elucidative mechanisms need to explain the observed high magnitude of magnetoresistivity, such as polaronic effects, intrinsically inhomogeneous states and Jahn–Teller (JT) distortion [10–15].

According to the literature, it was reported that the partial substitution of La^{3+} by Tb^{3+} in $La_{0.7}Ca_{0.3}MnO_3$ causes sharp changes in the magnetic and electrical properties [16]. Also, the substitution by Y^{3+} or Pr^{3+} decreases the Curie temperature and enhances the resistivity of the samples [17,18]. The effect of Eu doping at A-site of manganites has been studied by many groups. In fact, Reddy et al. [19] showed that the Eu doped $La_{0.67-x}Eu_xCa_{0.33}MnO_3$ compounds with $x \leq 0.29$ exhibit lower Curie and insulator–metal transition temperatures with respect to the undoped sample in addition to possessing CMR property. Similar results have been reported too by several groups in Sm, K and Gd doped CMR manganites [20–22].

In this work and for a better understanding of the effect of Eu doping on structural and magneto-electrical properties of lanthanum based compounds, we have elaborated and characterized two samples of nominal compositions $La_{0.7-x}Eu_xCa_{0.3}MnO_3$ ($x = 0$ and 0.1). This is a typical example of a spin-disorder system and is suitable for studying the physical mechanisms and their relative evolutions. In addition to structural changes seen by this kind of doping, an increase in resistivity and a decrease of the metal–insulator transition temperature are revealed. As observed in recent studies [23–26], a minimum in resistivity was also obtained in the present work. In order to explain the origin of this behaviour, the experimental data is analyzed by using different mechanisms, such as spin dependent transport mechanism, Kondo like scattering and quantum correction to conductivity [27–29]. Although there are many works including the physical mechanism of the low temperature resistivity minimum, it needs further clarifications for a deeper understanding. At high temperatures, the

* Corresponding author. Tel.: +90 374 2541000; fax: +90 374 2534642.
E-mail address: terzioglu_c@ibu.edu.tr (C. Terzioglu).

0925-8388/$ – see front matter © 2011 Elsevier B.V. All rights reserved.
doi:10.1016/j.jallcom.2011.01.008

semi-conducting-like curve resistivity is fitted by the small polaron hopping (PH) model and the nature of the conduction is inferred.

2. Experimental

Bulk samples of $La_{0.7}Ca_{0.3}MnO_3$ and $La_{0.6}Eu_{0.1}Ca_{0.3}MnO_3$ were prepared by the conventional solid-state reaction method. The highly purified powders (99.9%) of La_2O_3, Eu_2O_3, $CaCO_3$ and MnO_2 are mixed in stoichiometric ratios, ground and calcined at 1173 K for 20 h. The remaining black powder was ground, pelletized and sintered for another 20 h at 1273 K with two intermediate grindings. Finally the obtained pellets are reground, pelletized and annealed at 1423 K for 10 h. The phase purity and crystal structure are examined by X-ray diffraction (XRD) using a D 8-Advance Bruker type diffractometer with Cu Kα radiation (λ = 1.5418 Å). The cell parameters are refined by use of JANA2006 software [30]. Microstructure examination of the samples is done by use of a Philips XL30 SFEG scanning electron microscope (SEM). Resistivity measurements are carried by the standard four probe technique on a He gas contact crycooler and superconducting coil magnet in different applied fields (0–7 T) over a temperature range 5–300 K. The magnetoresistance (MR) ratio is defined by:

$$\mathrm{MR}\ (\%) = \frac{\left|\rho(0) - \rho(H)\right|}{\rho(0)} \times 100, \quad (1)$$

where $\rho(0)$ and $\rho(H)$ are the measured resistivity without and with magnetic field, respectively.

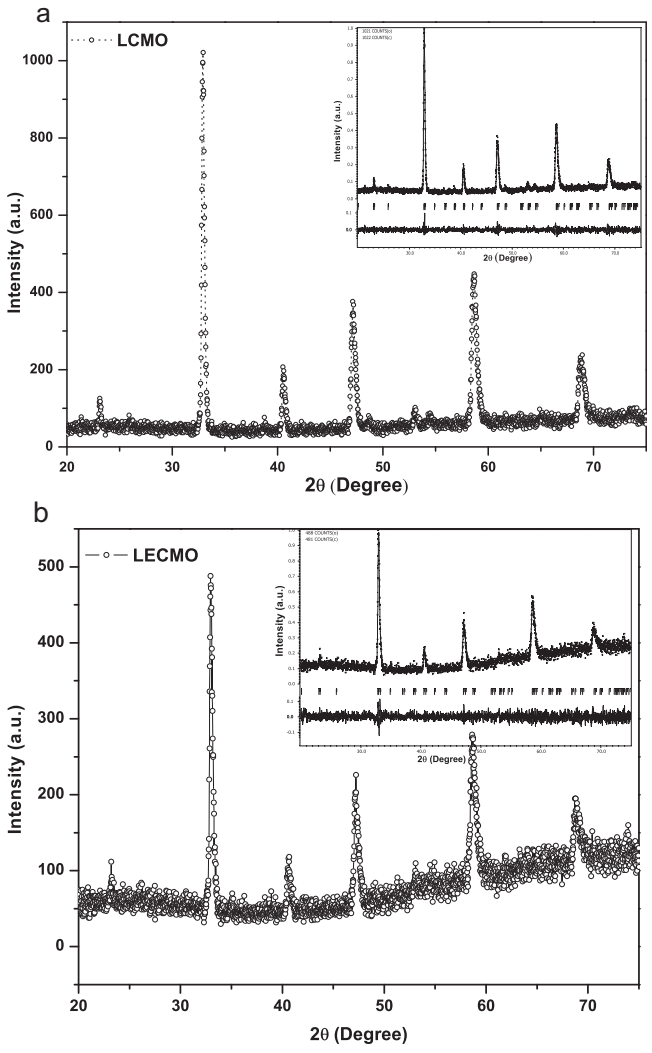

Fig. 1. XRD patterns of the (a) $La_{0.7}Ca_{0.3}MnO_3$ and (b) $(La_{0.6}Eu_{0.1})Ca_{0.3}MnO_3$ (b). The insets show the superposition of the observed (dots) and the calculated (line) patterns. The bars just below the patterns are the Bragg positions and the lines at the bottom correspond to the difference.

3. Results and discussion

3.1. Structural aspects

The X-ray diffraction patterns of all samples were recorded at room temperature and are displayed in Fig. 1. Significant peaks that representing different *h k l* planes had been observed from the XRD patterns of LCMO and LECMO. One can see from the XRD patterns that the samples are well crystallized in a single phase since no extra peaks are detected. The observed lines of both samples belong to the simple-perovskite-type structure and are in agreement with previous results [31]. The superposition of the observed and calculated XRD patterns for both samples is shown in the insets of Fig. 1. The refinement of cell parameters was done in the orthorhombic system with *Pbnm* space group. Details of the procedure are as follows. The experimental intensities are fitted by use of pseudo-Voight function. A 36 terms of Legendre polynoms was used to describe the backround and the Simpson method was applied for the asymmetry correction. The obtained cell parameters as well as the agreement factors (R_p, R_{wp}) and the goodness of the fit (GOF) are listed in Table 1. As can be seen, the GOF values for LCMO and LECMO were found to be 1.07 and 1.08, respectively. It is well known that when GOF value is ∼1, the fitting is expected to be very good. The decrease of the cell volume with doping may be associated to the low ionic radii of Eu^{3+} (1.120 Å) than that of the substituted La^{3+} (1.216 Å) [32].

The representative SEM micrographs with 3000× magnification obtained at room temperature for LCMO and LECMO composites are shown in Fig. 2. Overall, SEM images show that various sizes of grains are randomly distributed and uniform grain size with significant pores is formed for both samples that one can observe clear grain boundaries.

3.2. Electrical behaviour and magnetoresistance

The evolution of the resistivity with temperature under different magnetic applied fields is plotted in Fig. 3. Both samples are found to exhibit a metal–insulator transition in the studied temperature range. Compliant with other systems previously studied [19,33,34], the metal–insulator transition temperature T_p is found to decrease with Eu doping from 194 to 165 K (Table 1). Also and as it can be seen from the same figure, the resistivity of the doped sample is twice larger than that of the undoped one. This improvement of conductivity could be associated to a successive substitution of Eu^{3+} at A-site (La^{3+}) which reduces the value of $\langle r_A \rangle$. Consequently, $\langle r_A \rangle$ becomes too small to fill the space in the cube centers, and the oxygen tends to move towards the center, reducing the d_{A-O} and d_{Mn-O} bond distances. This leads to a distortion in the lattice, and further a deviation in the Mn–O–Mn bond angle (θ) from 180° which provides a local trap for e_g electrons, possibly causing phase or domain separation. Moreover, the hopping amplitude of charge

Table 1
Experimental data of LCMO and LECMO.

Sample	$La_{0.7}Ca_{0.3}MnO_3$	$(La_{0.6}Eu_{0.1})Ca_{0.3}MnO_3$
Sample code	LCMO	LECMO
Ionic radii (Å)	1.216	1.12
a (Å)	5.412(1)	5.379(2)
b (Å)	5.445(1)	5.447(1)
c (Å)	7.711(1)	7.706(1)
V (Å)^3	227.2(1)	225.8(1)
R_p, R_{wp} (%)	9.61,12.54	9.24,11.80
GOF	1.07	1.08
Space group	*Pbnm* (N°62)	*Pbnm* (N°62)
T_p (K)	194	165
MR (%) around T_p for 7 T field	44	47

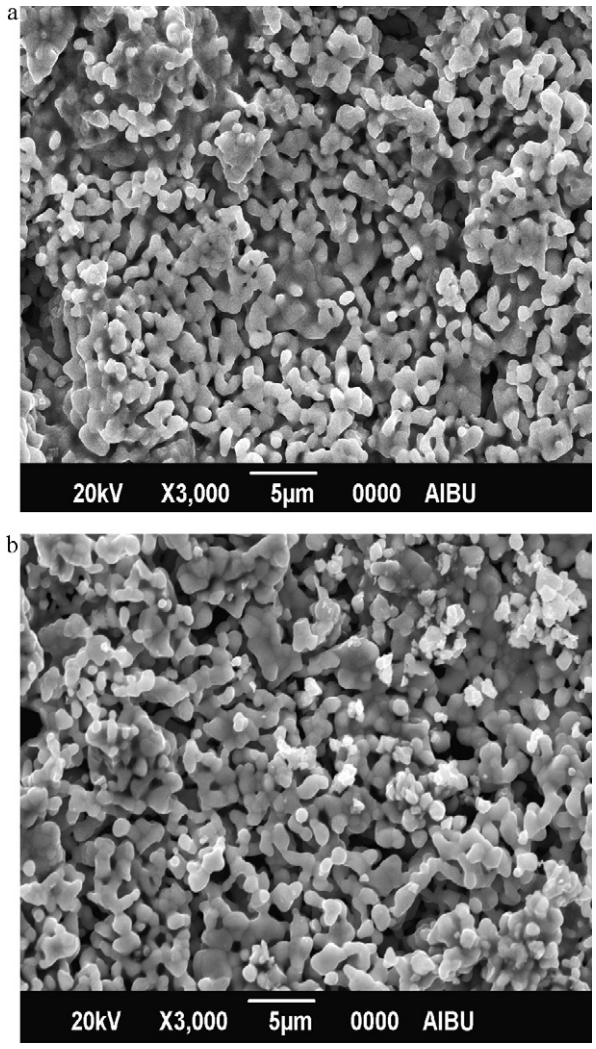

Fig. 2. SEM images of LCMO (a) and LECMO (b).

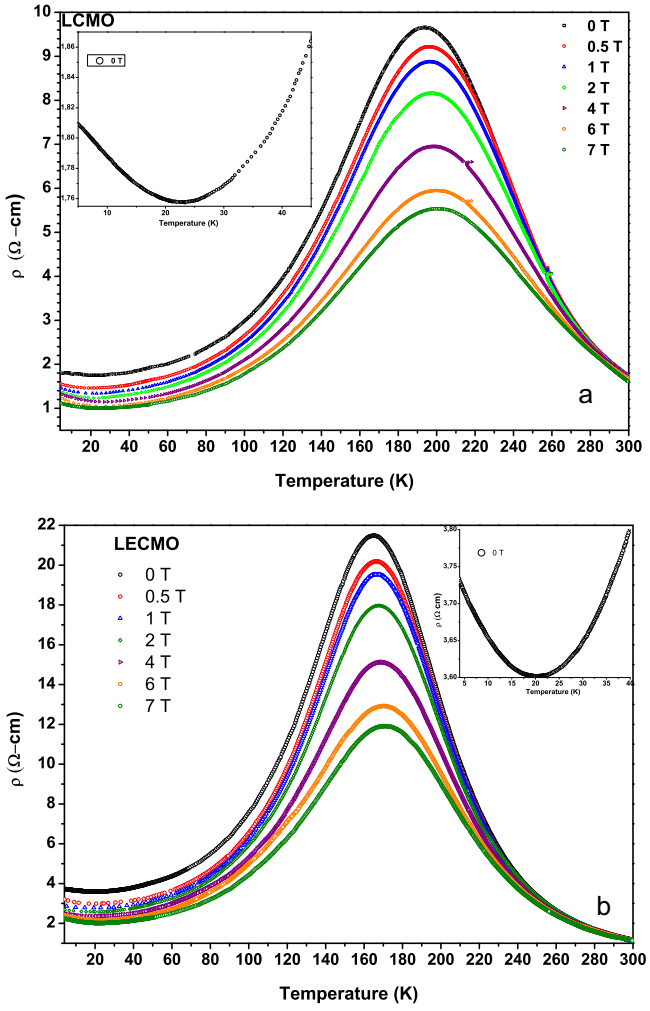

Fig. 3. Temperature dependence of resistivity under different magnetic fields for LCMO (a) and LECMO (b).

carriers between Mn^{3+} and Mn^{4+} naturally decreases as θ becomes smaller than 180°, leading to local lattice distortions of the MnO_6 octahedra. By consequence, the tendencies of charge localization increase due to the reduction in the mobility of the carriers. Due to that, the value of T_p is expected to decrease with decreasing $\langle r_A \rangle$ [33,35].

In zero field measurements of resistivity one can see from Fig. 3 that with decreasing temperature, the resistivity (ρ) increases up to metal–insulator transition temperature (T_p) and then decreases on further decrease of temperature and finally reaches a minimum value at about 20 K for LECMO and 24 K for LCMO. On further decrease of temperature below T_{min}, ρ is found to increase rapidly and the behaviour is a characteristic feature of an insulator [36]. In contrast with the normally observed metallic behaviour in the ferromagnetic region, the samples of present investigations are found to exhibit insulating behaviour. An obvious example can be seen in the insets of Fig. 3 for 0 T. In fact a similar type of behaviour was reported earlier in other kinds of materials [28,37,38]. Moreover, when the magnetic field is increased from 0 to 7 T, the maximum of the resistivity decreases from 21.5 to 11.8 Ω cm and from 9.7 to 5.5 Ω cm for LECMO and LCMO, respectively. At the same time, the transition temperature T_p shifts towards high temperature region by an amount of 10 K for both samples. This may be due to the fact that the applied magnetic field delocalizes the charge carriers by causing local ordering of the electron spins. Due to this ordering, the ferromagnetic metallic (FMM) state might have suppressed the paramagnetic insulating (PMI) regime resulting in increasing T_p values under the influence of magnetic field [39]. Further, T_{min} is found to shift towards low temperature region with increasing magnetic field. The resistivity upturn below T_{min} is also found to suppress with increasing magnetic field. The origin of this resistivity minimum at low temperatures could be associated to competition between the weak localisation effect, electron–electron scattering process and electron–phonon scattering process [40].

As the MR is a fundamental property of manganites, its percentage of the samples has been calculated using Eq. (1). Its evolution with temperature under an applied magnetic field of 7 T is shown in Fig. 4. The obtained values around T_p are given in Table 1. For both samples, the largest MR is observed around T_p and remains still remarkable even at the lowest temperatures. A maximum of 47% and 44% is obtained for the doped and undoped samples, respectively. The doping with Eu increases the magnetoresistance of $La_{0.7}Ca_{0.3}MnO_3$ system which is consistent with the same content of yttrium doped system [18]. Fig. 5 shows the variation of MR as a function of the applied magnetic field (from −4 to 4 T) at different temperatures. At low temperatures (≤100 K), the MR in the field below 1 T increases sharply with the increase of the applied field and shows the general behaviour of the polycrystalline samples with a large low-field MR [41,42]. After this value (H > 1 T), a

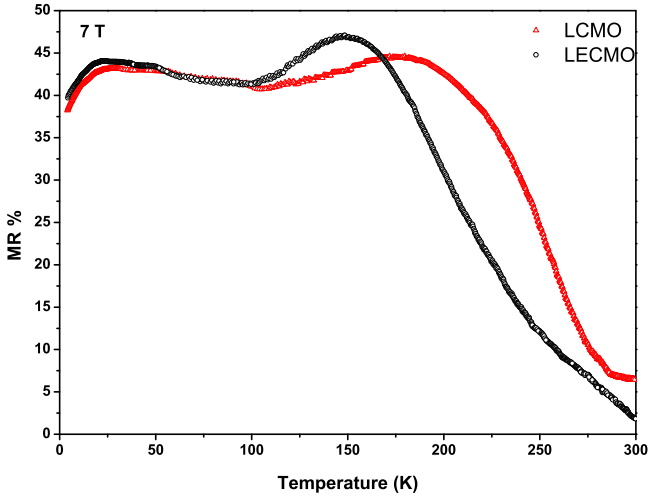

Fig. 4. MR (%) vs. temperature plots of the LCMO (△) and LECMO (○) samples in a field of 7 T.

slower variation of MR with H is observed. On the contrary, the variation of MR with H is quasi-linear at high temperatures. At 4 T and for all temperatures below T_p, the doped sample exhibits the highest value of MR.

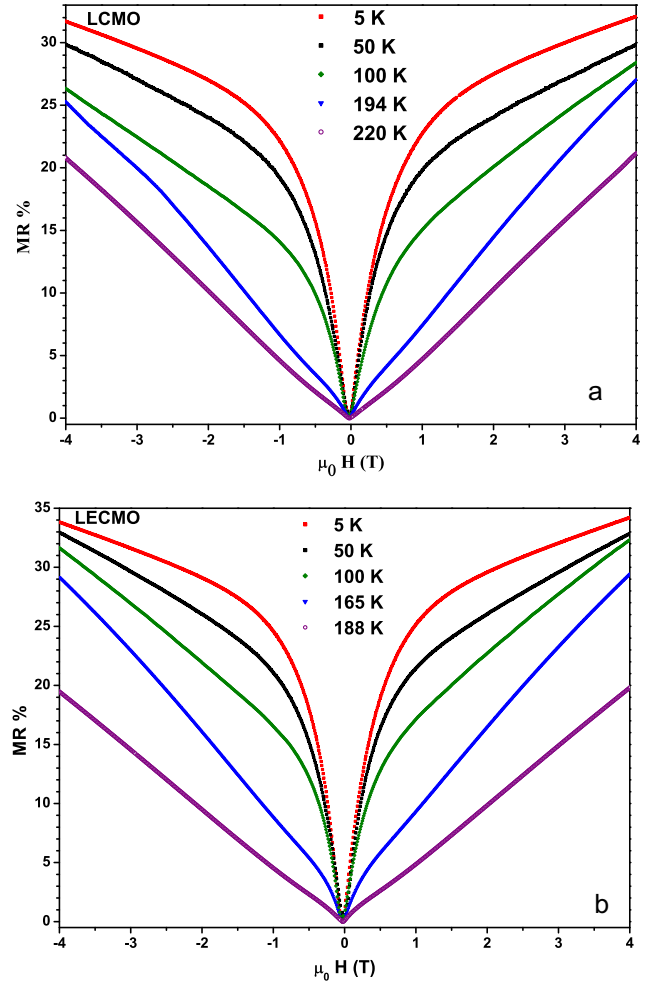

Fig. 5. MR (%) vs. magnetic field at different temperatures for LCMO (a) and LECMO (b).

3.3. Low-temperature behaviour

In spite of nearly two decades of intense work on CMR materials, the variation of resistivity at low temperatures ($T < T_p$) and relative strengths of the different scattering mechanisms originating from different contributions are not yet understood throughly. Therefore, in order to explain the origin of the low temperature resistivity upturn, the experimental data have been analyzed using the following empirical equation [24].

$$\rho(T) = \rho(0) + \rho_2 T^2 + \rho_{4.5} T^{4.5} + \rho_e T^{1/2} - \rho_s \ln T + \rho_p T^5 \quad (2)$$

where ρ_0 arises due to grain or domain boundaries. As the polycrystalline materials contain grains, grain boundaries and their significant contribution to the resistivity is proved in microwave measurements [43] and hence term ρ_0 will play a major role in the conduction process. On the other hand $\rho_2 T^2$ indicates the electron–electron scattering, while $\rho_{4.5} T^{4.5}$ is attributed to two magnon scattering processes. The last three terms are based on strong correlated effect in manganites; $\rho_e T^{1/2}$ takes care of the contributions from correlated electron–electron interactions, while $\rho_s \ln T$ represents the contributions due to Kondo-like spin dependent scattering. $\rho_p T^5$ term is due to electron–phonon interactions. The experimental resistivity data of present investigation were fitted to Eq. (2) and the best fit figures at 0 T and 7 T are shown in Fig. 6. It can be seen from the figures that the theoretical and the experimental curves match well. The fit parameters obtained for both curves are tabulated in Table 2. One finds from the table that all the parameters are found to decrease with increasing magnetic field (except ρ_s for LCMO) whereas they all increase with Eu doping. The observed behaviour may be explained as follows: when the magnetic field increases, the domain enlarges reducing the value of

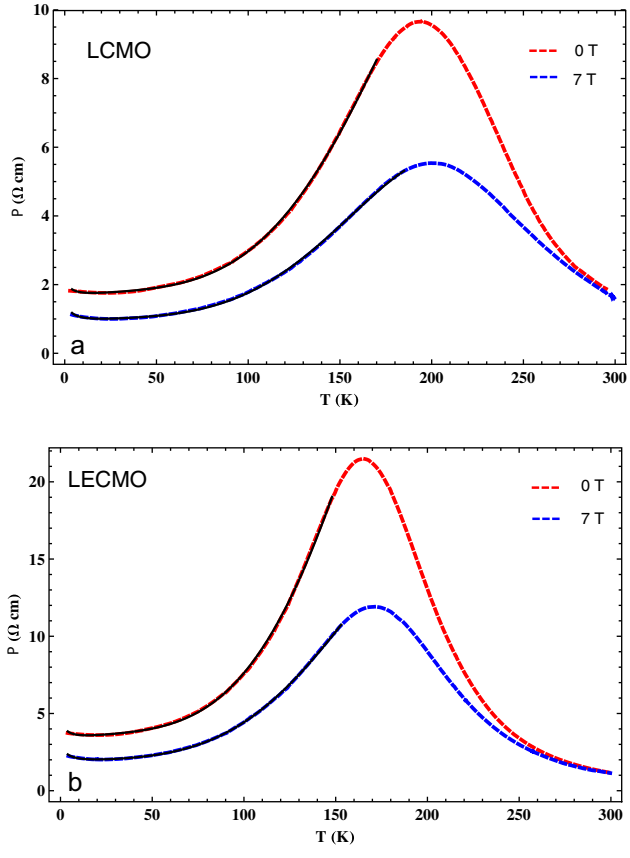

Fig. 6. Theoretical fit of low temperature resistivity data for LCMO (a) and LECMO (b).

Table 2
Best fit parameters of low temperature resistivity data.

Sample code	ρ_0 (Ω cm)		ρ_2 ($\times10^{-6}$ Ω cm/K^2)		$\rho_{4.5}$ ($\times10^{-9}$ Ω cm/K$^{4.5}$)		ρ_e (Ω cm/K$^{1/2}$)		ρ_s (Ω cm)		ρ_p ($\times10^{-10}$ Ω cm/K^5)	
	0 T	7 T	0 T	7 T	0 T	7 T	0 T	7 T	0 T	7 T	0 T	7 T
LCMO	1.96153	1.33255	34.8501	34.5014	2.70948	1.98308	0.165863	0.164143	0.309403	0.349267	1.58392	1.23866
LECMO	4.06633	2.66228	11.8577	9.27109	9.60308	5.28103	0.446547	0.278124	0.805593	0.626395	5.61911	3.31422

ρ_0. This may be related to the intrinsic properties of the system and does reflect CMR effect and disorder characteristics for the manganite system [41]. The reduction in ρ_2 and $\rho_{4.5}$ could be attributed to decrease in electron spin fluctuations in the presence of magnetic field. The increase in the last three terms indicates that the weak localization, electron–electron and electron–phonon scattering increase with Eu-doping, wherein disorder increases and the material becomes disordered.

3.4. High-temperature behaviour

In order to explain the variation of electrical resistivity with temperature in the high temperature insulating (semiconducting) regime (above the metal–insulator transition temperature T_p), the resistivity data is fitted by the adiabatic small polaron hopping (PH) model [44]. According to this model the expression of resistivity is given by the relation:

$$\frac{\rho}{T} = \rho_\alpha \exp\left(\frac{E_A}{k_B T}\right), \quad (3)$$

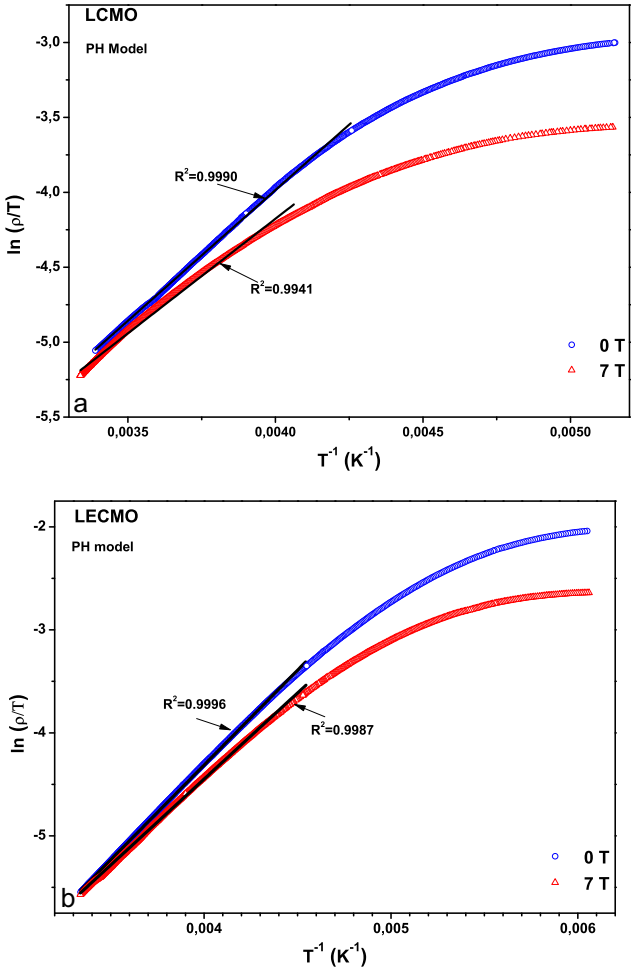

Fig. 7. Theoretical fit of high temperature resistivity data for LCMO (a) and LECMO (b).

Table 3
Fitting parameters of the PH model for LCMO and LECMO.

Sample code	H (T)	R^2	E_A (meV)	ρ_α ($\times10^{-6}$ mΩ cm/K)
LCMO	0	0.9990	150.39	17.288
	7	0.9942	131.84	33.765
LECMO	0	0.9996	158.65	8.4943
	7	0.9988	143.97	14.658

where E_A represents the activation energy and $\rho_\alpha = 2k_B/3ne^2a^2\nu$ is the residual resistivity. Here k_B is Boltzmann's constant, e is the electronic charge, n is the density of charge carriers, a is site-to-site hopping distance, and ν is longitudinal optical phonon frequency. The resistivity curves of the samples are plotted as $\ln(\rho/T)$ versus $(1/T)$ at 0 and 7 T (Fig. 7). Applying the PH model, we have calculated the values of activation energy E_A, and the fitting parameters for this model are presented in Table 3. One can see from the table that the activation energies are decreased by application of the magnetic field. This behaviour may be attributed to a reduction of the charge localization.

4. Conclusion

In summary, the structural and magneto-electrical properties of bulk $(La_{0.7-x}Eu_x)Ca_{0.3}MnO_3$ ($x = 0$ and 0.1) samples are presented. The Eu doping causes a decrease of the metal–insulator transition temperature T_p from 194 to 165 K and makes the resistivity twice larger. A maximum of magneto-resistance of 44% and 47% is observed at a magnetic field of 7 T for the undoped and doped samples, respectively. Moreover, these values are observed around their T_p and remains still remarkable even at the lowest temperatures. It has also been concluded that the electrical conduction mechanism at low temperatures ($T < T_p$) can be explained by a theory based on Kondo-like spin dependent scattering, electron–electron, electron–phonon and electron–magnon scattering while the adiabatic small polaron hopping machanism can be used in the high temperature ($T > T_p$) regime.

References

[1] J.M.D. Coey, M. Viret, S. von Molnar, Adv. Phys. 48 (1999) 167.
[2] D.H. Manh, P.T. Phong, T.D. Thanh, L.V. Hong, N.X. Phuc, J. Alloys Compd. 491 (2010) 8.
[3] P.K. Siwach, H.K. Singh, O. Srivastava, J. Phys.: Condens. Matter 20 (2008) 273201.
[4] Md.M. Seikh, L. Sudheendra, C.N.R. Rao, J. Solid State Chem. 177 (2004) 3633.
[5] J. Mira, J. Rivas, L.E. Hueso, F. Rivadulla, M.A. López Quintela, M.A. Señarís Rodríguez, C.A. Ramos, Phys. Rev. B 65 (2001) 024418.
[6] L. Hueso, N.D. Mathur, Nature 427 (2004) 303.
[7] S.L. Yuan, J.Q. Li, Y. Jiang, Y.P. Yang, X.Y. Zeng, G. Li, F. Tu, G.Q. Zhang, C.Q. Tang, S.Z. Jinet, Phys. Rev. B 62 (2000) 5313.
[8] M.T. Causa, M. Tovar, A. Caneiro, F. Prado, G. Ibanez, C.A. Ramos, A. Butera, B. Alascio, X. Obradors, S. Pinol, F. Rivadulla, C. Vazquez-Vazquez, M.A. Lopez-Quintela, J. Rivas, Y. Tokura, S.B. Oseroff, Phys. Rev. B 58 (1998) 3233.
[9] C. Zener, Phys. Rev. 81 (1951) 440.
[10] C. Sen, G. Alvarez, E. Dagotto, Phys. Rev. B 70 (2004) 064428.
[11] L. Pi, M. Hervieu, A. Maignan, C. Martin, B. Raveau, Solid State Commun. 126 (2003) 229.
[12] N. Panwar, V. Sen, D.K. Pandya, S.K. Agarwal, Mater. Lett. 61 (2007) 4879.
[13] A.J. Millis, P.B. Littlewood, B.I. Shraiman, Phys. Rev. Lett. 74 (1995) 5144.
[14] A.P. Ramirez, J. Phys.: Condens. Matter 9 (1997) 8171.
[15] P.G. de Gennes, Phys. Rev. 118 (1960) 141.

[16] J.M. DeTeresa, J. Blasco, M.R. Ibarra, J. Garcia, C. Marguina, P. Algarabel, A. del Moral, Solid State Commun. 96 (1995) 627.
[17] H.Y. Hwang, S.W. Cheong, P.G. Radaelli, M. Marezio, B. Batlogg, Phys. Rev. Lett. 75 (1995) 914.
[18] G.M.B. Castro, A.R. Rodrigues, F.L.A. Machado, A.E.P. de Araujo, R.F. Jardim, A.K. Nigam, J. Alloys Compd. 369 (2004) 108.
[19] T.G. Reddy, P.Y. Reddy, V.R. Reddy, A. Gupta, M. Gupta, K.R. Reddy, Solid State Commun. 133 (2005) 77.
[20] G.H. Zheng, Z.X. Dai, Y.Y. Zhang, Y.P. Sun, J. Alloys Compd. 489 (2010) 348.
[21] M. Mazaheri, M. Akhavan, J. Magn. Magn. Mater. 322 (2010) 3255.
[22] J.H. Hao, Z.S. Li, H.K. Wong, Mater. Sci. Eng. B 83 (2001) 70.
[23] E. Syskasis, G. Choudalakis, C. Papastaikoudis, J. Phy.: Condens. Matter 15 (2003) 7735.
[24] M. Ziese, Phys. Rev. B 68 (2003) 132411.
[25] D. Kumar, J. Sankar, J. Narayan, R.K. Singh, A.K. Majumdar, Phys. Rev. B 65 (2002) 094407.
[26] T. Okuda, T. Kimura, Y. Tokura, Phys. Rev. B 60 (1999) 3370.
[27] N.V. Khiem, P.T. Phong, N.V. Dai, H.D. Chinh, D.H. Manh, L.V. Hong, N.X. Phucet, Mater. Lett. 63 (2009) 899.
[28] E. Rozenberg, M. Auslender, I. Felner, G. Gorodetsky, J. Appl. Phys. 88 (2000) 2578.
[29] P. Sheng, B. Abeles, Y. Arie, Phys. Rev. Lett. 73 (2006) 214425.
[30] V. Petricek, M. Dusek, L. Palatinus, Jana 2006, The Crystallographic Computing System, Institute of Physics, Praha, Czech Republic.
[31] ICDD-Powder Diffraction File, 460513, International Centre for Diffraction Data, 12 Campus Boulevard, Newtown Square, PA, USA.
[32] G.R. Turpu, A. Gupta, K.R. Reddy, J. Phys. D: Appl. Phys. 42 (2009) 145004.
[33] G. Venkataiah, V. Prasad, P. Venugopal Reddy, Solid State Commun. 141 (2007) 73.
[34] M. Xu, X. Hu, J. Yu, X. Cui, S. Zhang, Solid State Commun. 148 (2008) 217.
[35] S. Bhattacharya, R.K. Mukherjee, B.K. Chaudhuri, Appl. Phys. Lett. 82 (2003) 4101.
[36] S. Jin, T.H. Tiefel, M. McCromack, R.A. Fastnach, R. Ramesh, L.H. Chen, Science 264 (1994) 413.
[37] M. Auslender, A.E. Karkin, E. Rozenberg, G. Gorodetsky, J. Appl. Phys. 89 (2001) 6639.
[38] T. Sarkar, B. Ghosh, A.K. Raychaudhuri, T. Chatterji, Phys. Rev. B 77 (2008) 235112.
[39] G. Venkataiah, P.V. Reddy, Solid State Commun. 136 (2005) 114.
[40] L. Li, K. Nishimura, M. Fujii, K. Mori, Solid State Commun. 144 (2007) 10.
[41] Y. Xu, J. Zhang, G. Cao, C. Jing, S. Cao, Phys. Rev. B 73 (2006) 224410.
[42] H.Y. Hwang, S.-W. Cheong, N.P. Ong, B. Batlogg, Phys. Rev. Lett. 77 (1996) 2041.
[43] M. Dominguez, S.M. Bhagat, S.E. Lofland, J.S. Ramachandran, G.C. Xiong, H.L. Ju, T. Venkatesan, R.L. Greene, EuroPhys. Lett. 32 (1995) 349.
[44] M. Ziese, C. Srinitiwarawong, Phys. Rev. B 58 (1998) 11519.